Effects of composition of $PbTiO_3$ on optical properties of $(1-x)PbMg_{1/3}Nb_{2/3}O_3$-$xPbTiO_3$ thin films

K. Y. Chan, W. S. Tsang, C. L. Mak,* and K. H. Wong
Department of Applied Physics and Center of Smart Materials, The Hong Kong Polytechnic University, Hung Hom, Hong Kong SAR, China

P. M. Hui
Department of Physics, The Chinese University of Hong Kong, Shatin, Hong Kong SAR, China
(Received 18 November 2003; revised manuscript received 5 February 2004; published 16 April 2004)

Thin films of $(1-x)PbMg_{1/3}Nb_{2/3}O_3$-$xPbTiO_3$ (PMN-PT) with $x=0$, 0.1, 0.3, 0.35, and 0.4 have been fabricated on (001)MgO single-crystal substrates by pulsed laser deposition (PLD). X-ray diffraction (XRD), scanning electron microscopy (SEM), and atomic force microscopy (AFM) were employed to characterize the structural properties of these PMN-PT films. Our results show that these films possess excellent structural properties and are cube-on-cube grown on (001)MgO substrates. Spectroellipsometry (SE) was used to characterize the depth profiles, the microstructural inhomogeneities, including void and surface roughness, refractive indices and extinction coefficients of the films. In the analysis of the measured SE spectra, a double-layer Lorentz model with four oscillators was adopted to represent the optical properties of the PMN-PT films. In this model, the films were assumed to consist of two layers—a bottom bulk PMN-PT layer and a surface layer composed of bulk PMN-PT as well as void. Good agreement was obtained between the measured spectra and the model calculations. The film thickness measured by SEM is consistent with that obtained by SE while the root mean square (rms) surface roughness determined by AFM is also close to our fitted effective surface layer thickness obtained by SE. Our measurements show that the refractive indices of the PMN-PT films increase with $PbTiO_3$ contents. This dependence is consistent with our optical transmittance measurements which revealed that the energy band gaps of PMN-PT films decrease with increasing $PbTiO_3$ contents. The correlation between the energy band gap and the refractive index is discussed.

DOI: 10.1103/PhysRevB.69.144111 PACS number(s): 78.20.Bh, 78.40.−q

I. INTRODUCTION

Thin-film ferroelectrics offer unique physical characteristics that could dramatically improve the performance of many integrated optic devices. Potential applications include low-voltage electro-optic switching, compact low-threshold gain devices, and second-harmonic generation. $(1-x)PbMg_{1/3}Nb_{2/3}O_3$-$xPbTiO_3$ (PMN-PT) is a useful ferroelectric with many interesting properties. When x is ~ 0.1, PMN-PT has high dielectric constant, while at $x \sim 0.35$, it has a very large electro-optic coefficient. Obviously, the $PbTiO_3$ (PT) content largely affects both the optical and dielectric properties of PMN-PT. Studies have been reported on the refractive indices of a PMN single crystal,[1] 0.7PMN-0.3PT ceramic[2] and $PbTiO_3$ ceramic.[3] The values are 2.522, 2.598, and 2.668 at 633 nm, respectively. Bing *et al.*[4] further suggested that for the PMN-PT family, the refractive index increases with PT content due to the higher refractive index of pure PT as compared to that of pure $PbMg_{1/3}Nb_{2/3}O_3$ (PMN). To our knowledge, the dependence of refractive indices as well as extinction coefficients of PMN-PT thin films as a function of PT composition has not been reported. These optical constants of PMN-PT films, however, are of practical importance for advanced optical device applications of these PMN-PT films.

In this paper we report on the refractive indices and extinction coefficients of PMN-PT films of different PT contents measured by spectroellipsometry. PMN-PT films were grown on a MgO single crystal using the pulsed laser deposition (PLD) method. The choice of using the MgO substrate is based on the small lattice mismatch and the large difference in the refractive index between the PMN-PT film and the MgO substrate. The MgO single crystal has a lattice constant of 4.21 Å which is close to that of PMN-PT (4.02 Å).[5,6] The refractive index of 0.7PMN-0.3PT ceramic is 2.598 at 633 nm,[2] and this value is much larger than that of MgO (1.734) at 650 nm.[7] A larger refractive index difference between the film and substrate increases the amplitude of oscillations of ellipsometric spectra, and thus enhances the accuracy of ellipsometric measurements. After obtaining the extinction coefficient spectra of the films, the absorption coefficient spectra, and hence the band gaps of PMN-PT, were estimated. These estimated band gap values were compared to those values measured by optical transmittance measurements. Good agreement was found between the two sets of data. Finally, the effects of PT composition on the optical properties as well as the optical band gap of PMN-PT films are discussed.

II. EXPERIMENT

PMN-PT films were grown on (001)MgO single crystal substrates with PT content $x=0$, 0.1, 0.3, 0.35, and 0.4 by PLD using an ArF excimer laser. All the 25.4-mm-diam and 5-mm-thick cylindrical PMN-PT targets were fabricated from single phase PMN-PT powders pressed at 80 MPa and sintered at 900 °C for 10 h. Unless stated otherwise, the fol-

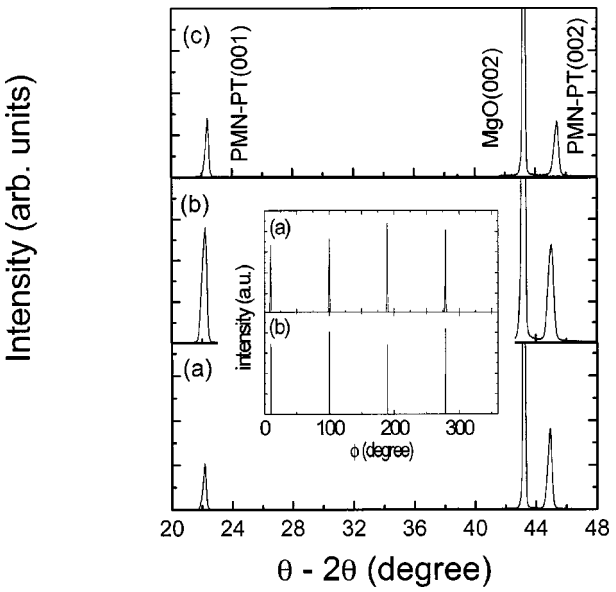

FIG. 1. X-ray diffraction patterns of (a) PMN, (b) 0.7 PMN-0.3PT, and (c) 0.6PMN-0.4PT films grown on MgO substrates with deposition temperature of 670 °C. The inset shows the XRD ϕ scans of (a) 0.7PMN-0.3PT(202) and (b) MgO(202).

lowing conditions for the deposition of PMN-PT films were employed in all cases. The PMN-PT films were deposited in a high vacuum chamber equipped with a rotating holder. The distance between the substrate and the target was kept at 5 cm throughout the experiment. Conditions of 670 °C substrate temperature, 200 mTorr ambient oxygen pressure, 6 Hz laser repetition rate, 4 J/cm^2 energy density, and 20 min deposition time were used. After deposition, the as-grown PMN-PT films were postannealed at the deposition temperature and pressure for 10 min. Afterwards, the films were cooled naturally to room temperature. X-ray diffraction (XRD Philip PW3710) using Cu K_α radiation, scanning electron microscopy (SEM, Leico, Stereoscan440), and atomic force microscopy (AFM) were employed to characterize the structural properties of our PMN-PT films. For optical analyses, spectroellipsometry (SE) measurements were carried out by a variable angle spectroscopic phase-modulated ellipsometer (Jobin Yvon UVISEL) at photon energy between 0.75 eV and 3.5 eV with a 0.01-eV interval. An incidence angle of 70° was used throughout our measurements. Finally, optical transmittance measurements were carried out by a two-beam spectrophotometer (Shimadzu UV-2101).

III. RESULTS AND DISCUSSION

The XRD θ–2θ profiles of the PMN-PT/MgO films with different PT contents are shown in Fig. 1. Highly oriented PMN-PT films of perovskite phase are observed in all PT contents. The out-of-plane lattice constants calculated from the diffraction angles of (002) peak of PMN-PT films with $x=0$, 0.1, 0.3, 0.35, and 0.4 are 4.03, 4.02, 4.02, 4.02, and 4.00 Å, respectively. The full width at half maximum (FWHM) of the rocking curves for all PMN-PT films are ~0.8°. To give an idea of the instrumentation limit of our XRD machine, the FWHM value for single-crystal MgO substrate is $\leqslant$0.2°. XRD ϕ scans of the (202)PMN-PT and (202)MgO were performed to confirm the epitaxy of our films. The inset of Fig. 1 shows a typical ϕ scan for the PMN-PT film with $x=0.3$. The peaks of PMN-PT and MgO are at the same position and separated by 90°. This clearly shows the fourfolded symmetry of both the film and the substrate. Our XRD results indicate that all PMN-PT films are cube-on-cube grown on (001)MgO substrates with an in-plane epitaxial relationship of (001)PMN-PT$\|$(001)MgO.

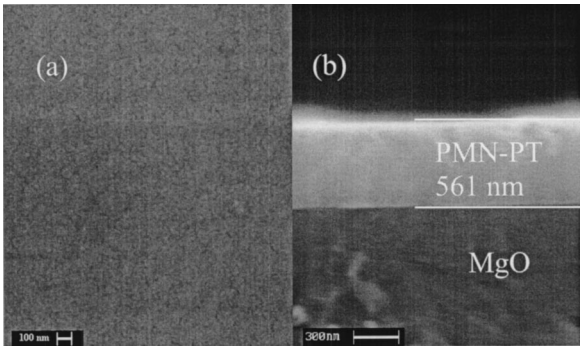

FIG. 2. SEM micrographs showing the (a) surface morphology and (b) cross section of a 0.65 PMN-0.35PT film grown on a MgO substrate.

Figure 2 shows the surface and cross-section SEM images of a PMN-PT film with $x=0.35$. The surface, in general, is smooth and crack-free as observed in SEM micrographs, while the film and the substrate are easily distinguished in the cross-section SEM image. All the films show similar features. The thickness of this 0.65PMN-0.35PT film is ~561 nm and is close to the value obtained by SE. The root mean square (rms) roughness of the film was found to be ~3.9 nm using AFM. This value is similar to that obtained by SE ($d_2=3.2$ nm). Figure 3 shows a typical AFM image of our 0.65PMN-0.35PT films. As shown by the data in Table I, all films have similar features with a small rms roughness.

Figure 4 shows the ellipsometric spectra of experimental

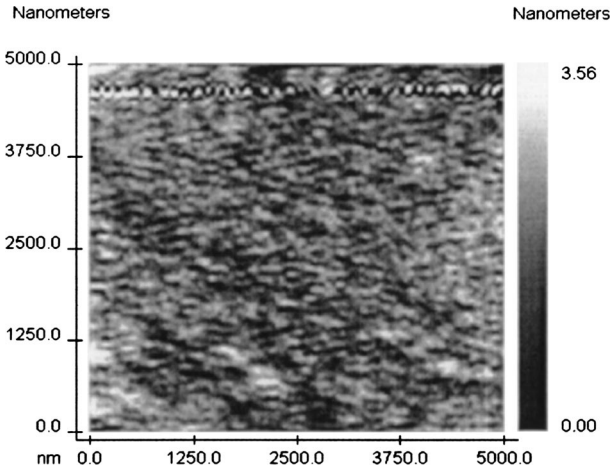

FIG. 3. AFM image of a 0.65 PMN-0.35PT film grown on a MgO substrate.

TABLE I. The physical parameters for different PMN-PT films obtained by SE, SEM, and AFM.

$(1-x)$PMN-xPT x	d_1 (nm)	d_2 (nm)	SEM $d=d_1+d_2$ (nm)	AFM d_2 (nm)	E_g (Trans) (eV)	E_g (Ellip) (eV)
0	621	4.0	657	4.3	3.63	3.53
0.1	517	3.8	480	3.8	3.60	3.52
0.3	580	7.5	535	7.6	3.55	3.51
0.35	538	3.2	561	3.9	3.54	3.50
0.4	907	11	850	9.8	3.54	3.46

and simulated ellipsometric angles I_S and I_C for a 0.7PMN-0.3PT film. Generally, SE measures the traditional ellipsometric angles ψ and Δ as a function of energy in the experiment. Here, the spectroscopic phase-modulated method was used. The incident light beam was polarized before reflecting from the sample. The reflected beam, after passing through a photoelastic modulator (M) and an analyzer (A), was dispersed by a monochromator and detected by a photomultiplier tube. The orientations (with respect to the plane of incidence) of the polarizer, modulator, and analyzer are denoted P, M, and A, respectively. The photoelastic modulator consists of a fused silica block sandwiched between piezoelectric quartz crystals oscillating at a frequency of ~50 kHz. This generated a periodic phase shift $\delta(t)$ between orthogonal amplitude components of the transmitted beam. The detected intensity has the general form

$$I(t)=I[I_0+I_S\sin\delta(t)+I_C\cos\delta(t)], \tag{1}$$

where I is a constant, and

$$\begin{aligned} I_0 &= 1-\cos 2\psi\cos 2A+\cos 2(P-M)\cos 2M(\cos 2A \\ &\quad -\cos 2\psi)+\sin 2A\cos\Delta\cos 2(P-M)\sin 2\psi\sin 2M, \\ I_S &= \sin 2(P-M)\sin 2A\sin 2\psi\sin\Delta, \\ I_C &= \sin 2(P-M)[\sin 2M(\cos 2\psi-\cos 2A)\sin\Delta \\ &\quad +\sin 2A\cos 2M\sin 2\psi\cos\Delta]. \end{aligned} \tag{2}$$

For a suitable choice of the angles A, M, and P, a simple determination of the ellipsometric angles from I_0, I_S, and I_C could be obtained. Throughout the experiment, we set

$$P-M=+45°, \quad M=0°, \text{ and } A=+45° \tag{3}$$

so that Eq. (2) can be rewritten as

$$\begin{aligned} I_0 &= 1, \\ I_S &= \sin 2\psi\sin\Delta, \\ I_C &= \sin 2\psi\cos\Delta. \end{aligned} \tag{4}$$

Therefore, the angles ψ and Δ can be determined accurately by measuring I_S and I_C.

The optical properties of an oxygen-octahedral ferroelectric are dominated by the BO_6 octahedra, which governs the low-lying conduction bands and the highest valence bands. This lowest energy oscillator is the largest contributor to the dispersion of the refractive index. Other ions in the structure contribute to the higher conduction bands and have a smaller effect on the optical properties of these ferroelectrics. In this paper a Lorentz oscillator model of the dielectric function with four oscillators,

$$\varepsilon(\omega)=\varepsilon_\infty+\sum_{j=1}^{4}\frac{S_j}{\omega_{oj}^2-\omega^2+i\gamma_j\omega} \tag{5}$$

has been used to describe the dominating interband oscillators of PMN-PT. The model parameters S_j, ω_{oj}, and γ_j are the oscillator strengths, resonance energies, and damping rate which gives the width of the resonance, respectively. The parameter ε_∞ represents the contributions at higher frequencies. Our initial analysis was based on a single-layer Lorentz model with four oscillators. Poor agreement, however, was found with the experimental data. In a subsequent analysis, we modified the single-layer Lorentz model into a double-layer Lorentz model (inset of Fig. 4). In this model, we assume that the films are composed of two layers—a bottom bulk PMN-PT layer and a surface layer consisting of bulk PMN-PT and voids. These voids in the surface layer were mainly caused by surface roughness. Let f_{v2} be the volume fraction of void (air) in the surface layer. The net optical constants of the mixed layer (PMN-PT+void) were calcu-

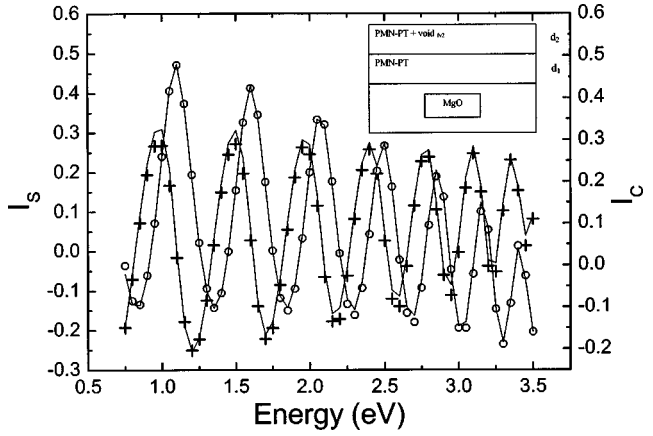

FIG. 4. Spectra of the ellipsometric parameters I_S and I_C as functions of energy from 0.7PMN-0.3PT films. The (+) and (○) are the measured I_S and I_C values, respectively, while the solid lines are model fitting. The inset shows the schematic picture of the double-layer Lorentz model.

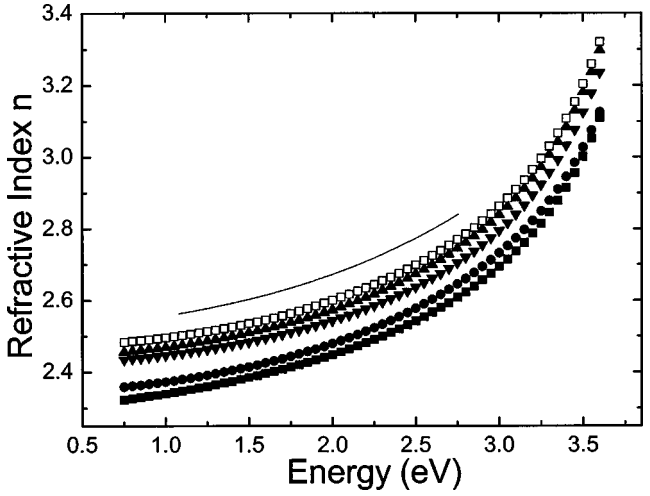

FIG. 5. Refractive indices n of the bottom layers of PMN (■), 0.9PMN-0.1PT (●), 0.7PMN-0.3PT (▼), 0.65PMN-0.35PT (▲), and 0.6PMN-0.4PT (□) films grown on MgO substrates. The solid line showing the refractive index of $PbTiO_3$ ceramics is obtained from Ref. 3.

lated by the Bruggeman effective-medium approximation. The reference data of the refractive index of the single crystal MgO is used for the substrate. Using this double-layer Lorentz model to analyze the data over the spectra range 0.75–3.5 eV, we obtained a good fit between the simulated values of I_S as well as I_C and the experimental data. The solid lines in Fig. 4 denote these results. Table I lists the physical parameters for different PMN-PT films obtained from our double-layer Lorentz model, SEM and AFM measurements.

Figures 5 and 6 show the refractive index n and the extinction coefficient k of PMN-PT films with different PT compositions as a function of energy obtained based on Eq. (5). In general, the extinction coefficients are fairly flat below 2.5 eV and increase more sensitively at higher energies. However, the refractive indices appear to be continuously increased nonlinearly over the entire range of energies with a more receptive increase at energies above 2.5 eV. This behavior is typical of an insulator or semiconductor in the range of energy near the band gap. Below the band gap, transmission dominates with a tiny extinction coefficient. As the band-gap energy is approached from below, both n and k increase when k approaches a resonance characterized by one of the oscillators in the Lorentz model. As the PT content increases, the refractive index of PMN-PT film increases. This is due to the smaller band gap and hence higher refractive index of PT as compared to that of PMN (shown in Fig. 5). The refractive index of PT ceramics[3] is also plotted in the figure for comparison. The dispersion profile of PT ceramics is very similar to those of our PMN-PT films of different PT contents. We notice that the refractive index of a PMN single crystal is larger than that of our PMN film. For example, the refractive indices of the PMN single crystal[2] and the PMN film are 2.522 and 2.469 at 633 nm, respectively. The slightly larger lattice constant of MgO implies that the epitaxial films take on a lower density than in the bulk. The presence of grain boundary, lower film density, and poor crystallinity in the films contribute to a reduced refractive index. Furthermore, grain size may also affect the refractive index. Further investigation is needed to unravel the dependence of the refractive index on grain size. Figure 5 shows that the extinction coefficient k of PMN-PT films increases sharply with energy for energies higher than 3.2 eV. The sharp increase in k signifies a change in the optical properties from dominantly transmission to absorption as the band-gap energy is approached. For PMN-PT films, the main contribution of optical loss comes from the band gap as well as grain boundary scattering. These mechanisms become increasingly important for photon energies near the band gap and for photon wavelengths comparable to the grain size of the films.[8,9]

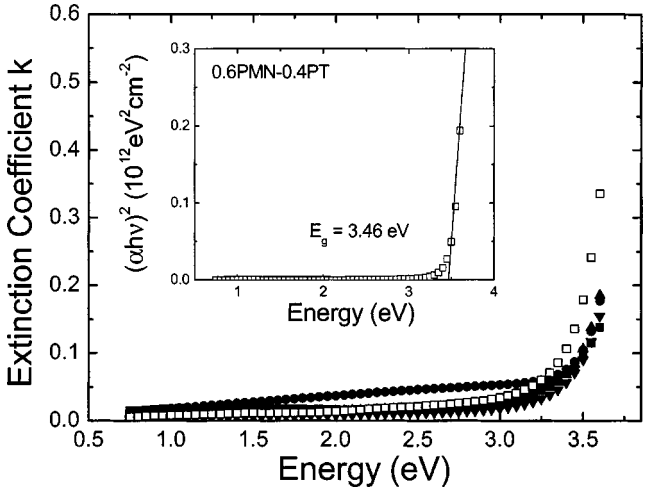

FIG. 6. Extinction coefficients k of the bottom layers of PMN (■), 0.9PMN-0.1PT (●), 0.7PMN-0.3PT (▼), 0.65PMN-0.35PT (▲), and 0.6PMN-0.4PT (□) films grown on MgO substrates. The inset shows the plot of $(\alpha h\nu)^2$ obtained from the fitted extinction coefficients against the energy for 0.6PMN-0.4PT films.

The dominating features in the optical properties of PMN-PT for energies below 3.5 eV come from the interband electronic transitions between the low-lying conduction bands and the upper valence bands. It is, therefore, useful to investigate the change in the band gap as the PT content changes. In order to determine the band-gap energy, the absorption coefficients α of the films were derived from the extinction coefficients using

$$\alpha = \frac{4\pi k}{\lambda}, \tag{6}$$

where k is the extinction coefficient and λ is the wavelength, as a function of energy. The band gaps of PMN-PT films were then deduced from the absorption coefficient α and the energy of the incident light $h\nu$ using the Tauc equation:[10]

$$(\alpha h\nu)^2 = B(h\nu - E_g), \tag{7}$$

where B is a constant and E_g is the band-gap energy. The relation $\alpha \propto \sqrt{h\nu - E_g}$ results from the joint density of states. By extrapolating the linear portion of the curve to zero, as shown in the inset of Fig. 6, band-gap energies were obtained for our PMN-PT films. The values are shown in Table I.

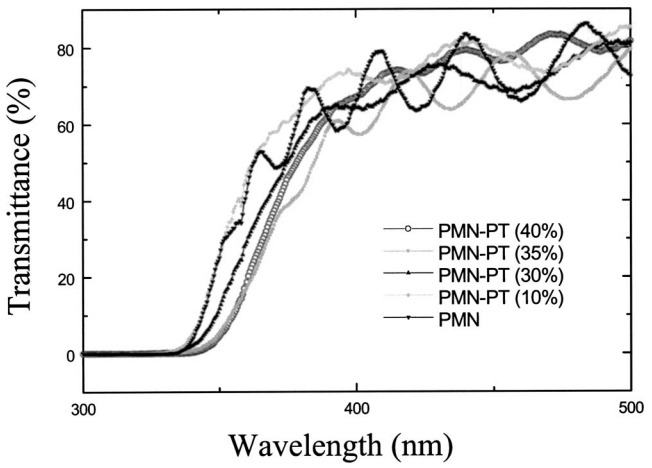

FIG. 7. Transmission spectra of PMN-PT films with different PT compositions.

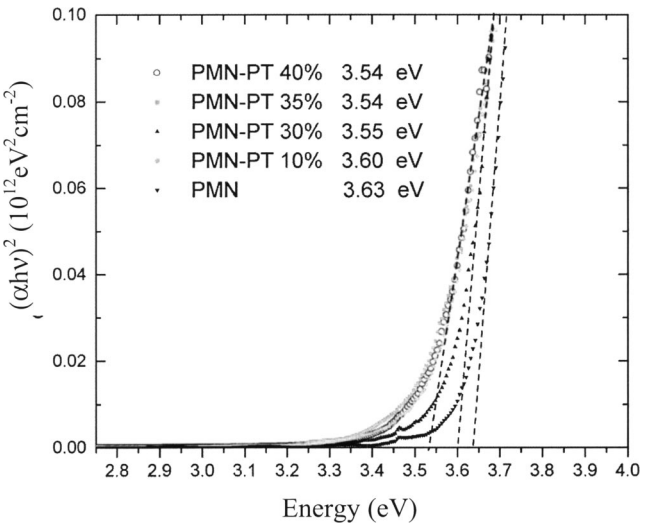

FIG. 8. Dependance of the absorption coefficients $(\alpha h\nu)^2$ on the photon energy obtained from the transmission spectra for PMN-PT films with different PT compositions.

In order to check the values of the band gap of PMN-PT films, optical transmittance measurements were also performed. Figure 7 shows the transmittance spectra of PMN-PT films grown on single crystal MgO. As the surface roughness is much smaller than visible wavelengths, the oscillating optical transmittance spectra result from multiple reflections. All the films show a good optical transmittance of ~80% in the visible region. The transmittance of the films decreases to zero near 350 nm due to interband transitions. Figure 8 shows the plot of $(\alpha h\nu)^2$ vs $h\nu$. By extrapolating the linear portion of the curve to zero, the band gap can then be identified. Results are listed in Table I. We notice that the two set of values of the band gap obtained by two different techniques take on very similar values. They both indicate that optical band-gap energy of PMN-PT is a composition-dependent parameter and decreases with the PT content.

IV. CONCLUSION

$(1-x)PbMg_{1/3}Nb_{2/3}O_3$-$xPbTiO_3$ (PMN-PT) films with $x=0$, 0.1, 0.3, 0.35, and 0.4 have been fabricated on MgO single-crystal substrates by PLD. SE was used to characterize the depth profile and refractive index of these films. It is found that the refractive index of PMN-PT films increases with the PT content. Meanwhile, the extinction coefficient of a PMN-PT film is small in the visible region and increases as the energy increases. The surface roughness and the film thickness obtained from a fitting using a double-layer Lorentz model are consistent with those measured by SEM and AFM. The transmittance results show that the optical band-gap energy of the PMN-PT film is composition dependent and decreases with the PT content. A reduced band gap with a higher PT content then leads to a higher refractive index at energies below the gap for films with a higher PT content.

ACKNOWLEDGMENTS

This research was partially supported by the Research Grant Council of the Hong Kong Special Administrative Region (PolyU5311/01P). K.Y.C. and W.S.T. were supported by the Hong Kong Polytechnic University.

*Corresponding author. Email author: apaclmak@polyu.edu.hk

[1] D. A. McHenry, J. R. Giniewicz, T. R. Shrout, S. J. Jang, and A. S. Bhalla, Ferroelectrics **102**, 160 (1990).
[2] D. A. McHenry, Ph.D. thesis, The Pennsylvania State University, 1992.
[3] *Landolt-Börnstein, Ferroelectric and Related Substances* (Springer-Verlag, Berlin, 1981), p. 16.
[4] Y. H. Bing, R. Guo, and A. S. Bhalla, Ferroelectrics **242**, 1 (2000).
[5] V. Nagarajan, C. S. Ganpule, B. Nargaraj, S. Aggarwal, S. P. Alpay, and A. L. Roytburd, Appl. Phys. Lett. **75**, 4183 (2000).
[6] M. Tyunina, J. Levoska, A. Sternberg, and S. Leppävuori, J. Appl. Phys. **86**, 5179 (1999).
[7] R. E. Stephens and I. H. Maalitson, J. Res. Natl. Bur. Stand. **49**, 249 (1952).
[8] M. J. DiDomenico and S. H. Wemple, J. Appl. Phys. **40**, 720 (1969).
[9] H. Y. Tian, W. G. Luo, X. H. Pu, X. Y. He, P. S. Qiu, A. L. Ding, S. H. Yang, and D. Mo, J. Phys.: Condens. Matter **13**, 4065 (2001).
[10] J. C. Tauc, *Optical Properties of Solids* (North-Holland, Amsterdam, 1972), p. 372.